Efficient spin-flip excitation of a nickelocene molecule

Maider Ormaza, Nicolas Bachellier, Marisa N Faraggi, Benjamin Verlhac, Paula Abufager, Philippe Ohresser, Loïc Joly, Michelangelo Romeo, Fabrice Scheurer, Marie-Laure Bocquet, et al.

Efficient spin-flip excitation of a nickelocene molecule

Maider Ormaza,*,† Nicolas Bachellier,† Marisa N. Faraggi,‡ Benjamin Verlhac,† Paula Abufager,¶ Philippe Ohresser,§ Loïc Joly,† Michelangelo Romeo,† Fabrice Scheurer,† Marie-Laure Bocquet,‡ Nicolás Lorente,‖ and Laurent Limot*,†

Université de Strasbourg, CNRS, IPCMS, UMR 7504, 67034 Strasbourg, France, Ecole Normale Supérieure, Département de Chimie, ENS-CNRS-UPMC UMR 8640, 75005 Paris, France, Instituto de Física de Rosario, Consejo Nacional de Investigaciones Científicas y Técnicas (CONICET) and Universidad Nacional de Rosario, Av. Pellegrini 250 (2000) Rosario, Argentina, Synchrotron SOLEIL, L'Orme des Merisiers, Saint-Aubin - BP 48, 91192 Gif-sur-Yvette, France, Centro de Física de Materiales CFM/MPC (CSIC-UPV/EHU), Paseo Manuel de Lardizabal 5, 20018 Donostia-San Sebastián, Spain, and Donostia International Physics Center (DIPC), Paseo Manuel de Lardizabal 4, E-20018 Donostia-San Sebastián, Spain

E-mail: ormaza@ipcms.unistra.fr; limot@ipcms.unistra.fr

Abstract

*To whom correspondence should be addressed

†Université de Strasbourg, CNRS, IPCMS, UMR 7504, 67034 Strasbourg, France

‡Ecole Normale Supérieure, Département de Chimie, ENS-CNRS-UPMC UMR 8640, 75005 Paris, France

¶Instituto de Física de Rosario, Consejo Nacional de Investigaciones Científicas y Técnicas (CONICET) and Universidad Nacional de Rosario, Av. Pellegrini 250 (2000) Rosario, Argentina

§Synchrotron SOLEIL, L'Orme des Merisiers, Saint-Aubin - BP 48, 91192 Gif-sur-Yvette, France

‖Centro de Física de Materiales CFM/MPC (CSIC-UPV/EHU), Paseo Manuel de Lardizabal 5, 20018 Donostia-San Sebastián, Spain

⊥Donostia International Physics Center (DIPC), Paseo Manuel de Lardizabal 4, E-20018 Donostia-San Sebastián, Spain

Inelastic electron tunneling spectroscopy (IETS) within the junction of a scanning tunneling microscope (STM) uses current-driven spin-flip excitations for an all-electrical characterization of the spin state of a single object. Usually decoupling layers between the single object, atom or molecule, and the supporting surface are needed in order to observe these excitations. Here we study the surface magnetism of a sandwich nickelocene molecule (Nc) adsorbed directly on Cu(100) by means of X-ray magnetic circular dichroism (XMCD) and density functional theory calculations (DFT), and show with IETS that it exhibits an exceptionally efficient spin-flip excitation. The molecule preserves its magnetic moment and magnetic anisotropy not only on Cu(100), but also in different metallic environments including the tip apex. Taking advantage of this robusteness we are able to functionalize the microscope tip with a Nc, which can be employed as a portable source of inelastic excitations as exemplified by a double spin-flip excitation process.

keywords: metallocene, spin-flip, magnetic anisotropy, tip functionalization, inelastic electron tunneling spectroscopy, X-ray magnetic circular dichroism, density functional theory

Recent advances in addressing and controlling the spin states of a surface-supported object –atom or molecule– have further accredited the prospect of quantum computing [1–3] and of an ultimate data-storage capacity. [4] Information encoding requires that the object must possess stable magnetic states, in particular magnetic anisotropy to yield distinct spin-dependent states in the absence of a magnetic field together with long magnetic relaxation times. [5–8] Scanning probe techniques have shown that inelastic electron tunneling spectroscopy (IETS) within the junction of a scanning tunneling microscope (STM) is a good starting point to study the stability of these spin states. STM-IETS allows for an all-electrical characterization of these states by promoting and detecting spin-flip excitations within the object of interest. [9–14] It can also provide an electrical control over these states, [15] simplifying the information readout process. As spin excitations need however to be preserved from scattering events with itinerant electrons, single objects are usually placed on non-metallic surfaces such as thin-insulating layers [7,8,16,17] or superconductors. [18]

In this work, we study how the spin of a sandwich molecule, nickelocene (Nc hereafter), is preserved in different environments and we explain the remarkably efficient spin-flip mechanism it exhibits. The chemical structure of nickelocene consists in a Ni atom sandwiched between two cyclopentadienyl rings (C_5H_5, Cp hereafter), endowing nickelocene with an electronic structure $(a_{1g})^2(e_{2g})^4(e_{1g})^2$ of spin $S = 1$ in the gas phase (Fig. 1a).[19] We prove that the molecular spin does not change upon adsorption on a metallic surface. In particular, by attaching a nickelocene to the tip apex of a STM, we show that two spin-flip excitations can be sequentially triggered, resulting in a large enhancement of the inelastic signal as illustrated by the IETS acquired above a surface-supported Nc. This unique situation can be achieved due to the chemical stability, the presence of magnetic anisotropy, the full preservation of the Nc spin on the tip apex, or more generally in a metallic environment, and the extremely efficient spin-flip excitation of this molecule.

To benchmark the electronic and magnetic properties of a Nc-terminated tip, we investigated first the nickelocene adsorption on a Cu(100) surface using a metal tip. The ring-shaped pattern visible in Fig. 1b indicates that individual nickelocene molecules bind to the surface through a Cp ring, while the other Cp ring is exposed to vacuum (see Methods for experimental details in the sample preparation). In particular, the Cp ring is centered on a hollow position of Cu(100) most likely adopting the D_{5h} symmetry (eclipsed configuration).[20] Figure 1c presents the differential conductance (dI/dV) versus bias (V) spectrum of an isolated Nc molecule by positioning the tip above the Cp ring, together with its numerical derivative. As shown, the dI/dV is small near zero bias (Fig. 1c) with symmetric steps (5 ± 1) times higher in conductance at an energy of $|3.2\pm0.1|$ meV (the uncertainty translates the tip-dependency observed). Since the vibrational excitations of nickelocene adsorbed on the surface can be *a priori* discarded in this energy range,[21] the differential conductance steps reveal the occurrence of spin-flip excitations within the molecule. In view of the spin 1 character predicted upon adsorption on Cu(100),[20] these excitations occur between the ground state (S=1, M=0) and the doubly-degenerated (S=1, M=$\pm$1) excited states of the

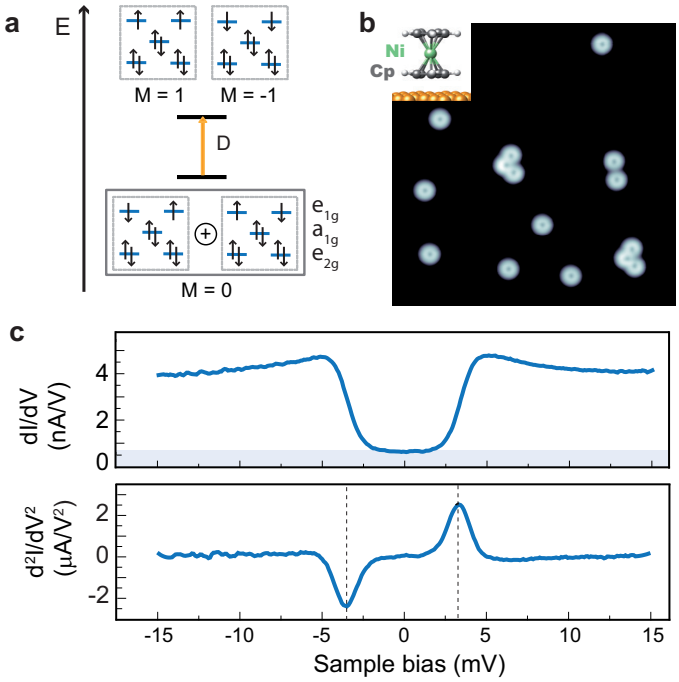

Figure 1: **Spin-flip excitations of a single Nc molecule.** (a) Energy diagram of the zero-field splitting for Nc. The ground state is S=1, M=0 and the degenerate excited states correspond to S=1, M=$\pm$1. (b) STM topography (14.5 $\times$ 14.5 nm^2, $-$15 mV, 20 pA) of Nc molecules adsorbed on a Cu(100) surface. Inset: Nc structure calculated by DFT. White, grey and green atoms correspond to H, C and Ni atoms. (c) Differential conductance spectrum and its derivative measured at 2.4 K acquired at 50 pA and $-$15 mV. The spectrum was measured by means of a lock-in amplifier using a modulation of 150 μV rms at 722 Hz. The d^2I/dV^2 versus V spectrum was obtained by numerically differentiating the dI/dV spectrum.

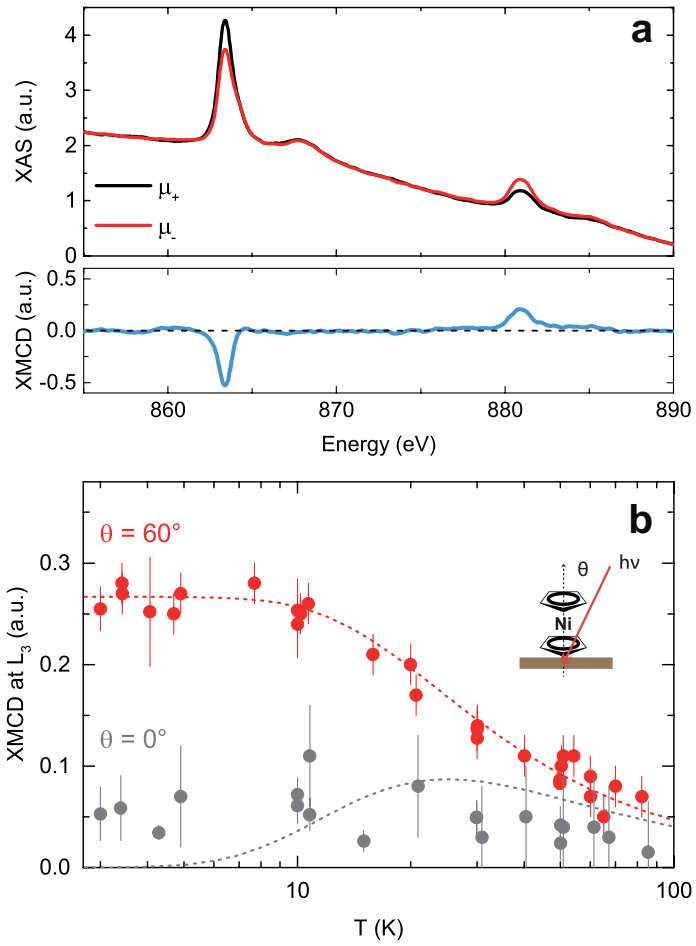

Figure 2: **XMCD measurements.** (a) Absorption spectra for left and right circularly polarized light and XMCD signal at the Ni $L_{2,3}$ edges in a 6.5 T magnetic field (60° off-normal) at 4.7 K for a collection of isolated molecules. (b) Maximum value of the L_3 XMCD signal for normal (grey circle) and 60° (red circle) off-normal incidence under a 6.5 T field as a function of temperature. The dashed lines correspond to simulations (see supplementary material) for a $S = 1$ system with a magnetic anisotropy of $D = 3.2$ meV; the simulations are scaled to the data by a factor 0.8. Note that the magnetic field is parallel to the X-ray beam.

molecule. The threshold energy observed in IETS corresponds then to a direct measurement of the longitudinal magnetic anisotropy energy, D (see Supporting Information).

To further characterize the magnetic origin of the excitation, we performed X-ray magnetic circular dichroism (XMCD) measurements in a magnetic field of 6.5 T on a collection of individual Nc molecules on Cu(100) (see Methods and fig. S1). The top panel of Fig. 2a shows X-ray adsorption spectra (XAS) recorded at the $L_{2,3}$ edges of Ni for left and right circularly polarized light. The panel below presents the difference between them, the so-called XMCD spectrum. Having a clear dichroic signal is already an indication of the magnetic character of nickelocene on Cu(100). Figure 2b shows the evolution of the signal maximum at the Ni L_3 edge as a function of the temperature for grazing (red dots, $\theta = 60°$) and normal (black dots, $\theta = 0°$) incidence of the applied magnetic field. At low temperature, the signal shows a clear angular dependence revealing the existence of an easy magnetization direction, more specifically of an easy plane perpendicular to the molecular axis. For the sake of comparison, we have simulated in Fig. 2b the magnetization of a $S = 1$ system under an external field of 6.5 T and possessing a magnetic anisotropy of $D = 3.2$ meV as determined by STM (see details of the simulation in the Supporting Information). Based on the XMCD results, we can assert that D is positive, implying that $M = 0$ corresponds to the ground state of nickelocene and the $M = \pm 1$ to the excited state.

The magnetic properties of isolated nickelocene turn out to be robust against external perturbations, possibly owing this behavior to the cyclic π^* orbital of the Cp rings sandwiching the Ni atom. This differentiates Nc from other systems reported so far[4,8,10,22] in which the local environment is a crucial factor determining the magnetic anisotropy and/or the spin. At higher coverages, for example, where Nc molecules self-assemble following a T-shaped geometry (Fig. 3b) typical for metallocenes,[20,23] no difference was observed in the IETS spectra of upstanding molecules within the layer (Fig. 3a). We have checked the impact of the surface symmetry by changing to Cu(111), also resulting in no difference for isolated or self-assembled nickelocene (Fig. 3a). Supporting these findings, we note that the spin 1

character and magnetic anisotropy are consistent with existing macroscopic measurements of Nc powder samples and crystallites [24,25] or matrix embedded samples[26] where D ranges from 3.17 meV to 4.16 meV; recent theoretical calculations for gas-phase Nc also predict D to be close to 5 meV.[27] In the following, we exploit such robustness to produce a portable source for spin-flip excitations by attaching a single nickelocene to the tip apex of the STM.

Similarly to previous works in which the STM tip was functionalized with atomic point-like probe-particles[28–35] or larger organic molecules,[36,37] we can transfer a Nc to our monoatomic tip apex by approaching the tip to the target molecule at -1 mV and 50 pA. This condition corresponds to a molecule-tip distance of 1.3 Å closer than the usual distances in the tunneling conditions in which we acquire the spectrum (-30 mV and 100 pA) (Figs. 3c and 3d). The tip functionalization is reversible, i.e., in the same way the molecule goes to the tip it can be released back to an atom on the surface (+1 mV), indicating that the molecule remains intact during the transfer process. Counter-images of the molecular tip acquired above a Cu atom (inset of Fig. 3d) confirm the presence of a nickelocene molecule. The half-moon shape that is observed can be easily assigned to a tilted Nc.[38] The nickelocene on the tip exhibits similar magnetic properties as previously seen for nickelocene on the surface (Figs. 3a and 4a). IETS acquired with such a molecular tip above the bare surface reveals a larger magnetic anisotropy of $D = (3.7 \pm 0.3)$ meV and conductance steps up to (9±1) times higher compared to the elastic conductance alone. The large step height observed experimentally in the conductance reflects a highly efficient spin-flip excitation that can be explained using a multichannel T-matrix approach due to the interference of two spin-channels with different symmetries, an effect not seen in previous experiments where only one channel prevails (see Supporting Information). The conductance above the inelastic threshold can be almost one order of magnitude larger than the elastic conductance, with some dependence on the STM tip employed for the measurements.

The magnetic properties of the molecular tip are computed by fully-relaxing a single nickelocene atop a Cu atom adsorbed on Cu(100). In Figs. 3e-g, the spin density of Nc in

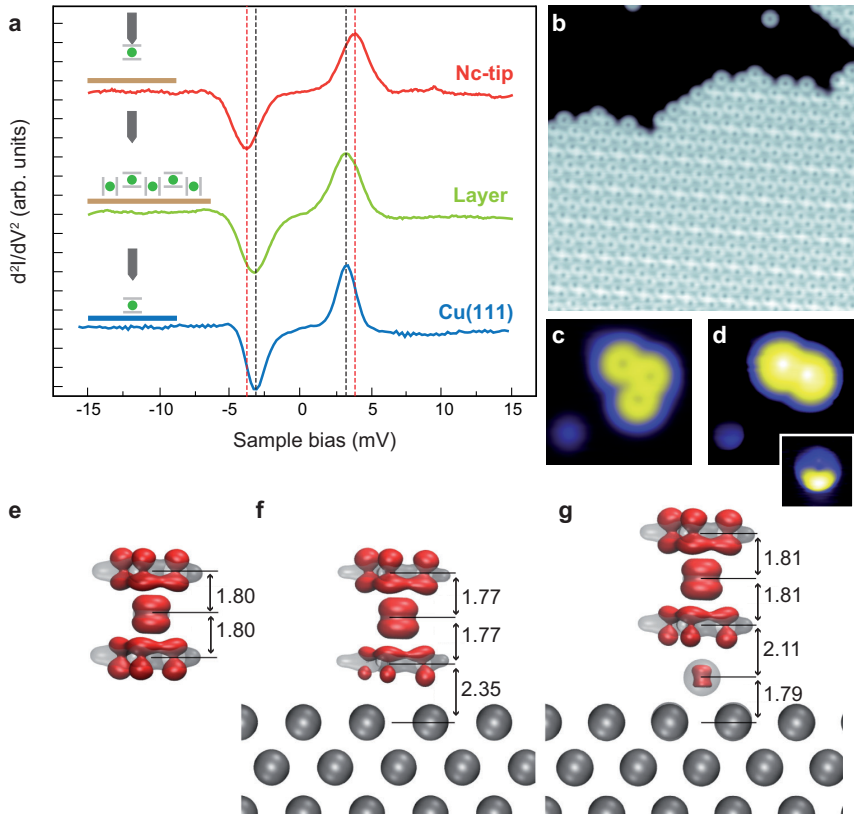

Figure 3: **Nc molecule in different environments.** (a) Second derivative of the differential conductance measured for three different environments: isolated Nc adsorbed on Cu(111) (in blue), Nc within the molecular self-assembled monolayer on Cu(100) (in green) and Nc adsorbed on the tip (in red). The spectra were taken with different feedback parameters and overlaid to highlight the different bias thresholds. (b) STM topography of the self-assembled Nc molecules forming a compact arrangement on Cu(100). Images (c) before and (d) after the transfer of Nc to the tip. The protrusion on the left corresponds to a Cu atom. With the Nc-terminated tip, the Cu atom exhibits a molecular pattern as visible in the inset of panel (d). (e-g) Calculated spin density (majority spin in red, negligible minority spin) and total electron density (grey transparent) of gas phase Nc with MAE= -1.54 meV (e), adsorbed Nc on Cu(100) with MAE= -1.27 meV (f) and adsorbed Cu-Nc on Cu(100) with MAE= -1.49 meV (g). A negative MAE corresponds to an easy plane, in other words to a positive value of D. The isosurface of the spin (total electron) density is 0.02 (1.3) electron per Å^3. Vertical heights are given in Å. Image parameters: (b) 18×18 nm^2, -20 mV, 20 pA, (c) and (d) 3.5×3.5 nm^2 (Inset of panel d: 1.5×1.5 nm^2).

three different environments –gas phase, adsorbed on Cu(100) and adsorbed on a Cu atom on Cu(100)– is shown together with the total electron density. The spin density is similar in the three cases showing that the molecule keeps a spin equal to 1. The spin density follows the density of the two degenerate frontier molecular orbitals, with weight on the d_{xz} and d_{yz} orbitals of the Ni atom and the π^* orbital of the Cps. For the Cu atom below Nc in Fig. 3g, there is a very small spin polarization that accounts for 2% of the total polarization. From both adsorbed cases, our calculations show that the surface polarizes with a minimum impact on the molecule and the molecular spin is the same in the three systems studied, obtaining a negligible value for the orbital moment of $0.1\mu_{\mathrm{B}}$. An inspection of the molecular geometry shows a small reduction of the Nc height (3.54 Å) upon adsorption on Cu(100) due to the depopulation of the anti-bonding frontier molecular orbital. This corresponds to a very small electron transfer (0.1 e^-) from the molecule to the surface. Interestingly, the charge transfer is reversed when Nc is on the Cu atom; the molecule charge increases by 0.14 electrons leading to a larger molecular height (3.62 Å). This translates into a different magnetic anisotropy energy (MAE), which in our case due to the axial symmetry and spin 1 character of the molecule corresponds to $|D|$ (see Supporting Information). Note that the differences between the calculated and the experimentally measured magnetic anisotropy values are due to limitations in the DFT calculations (see Methods). The MAE is smallest when the molecule is on the surface (Fig. 3f, -1.27 meV) and recovers the gas phase value (Fig. 3e, -1.54 meV) when adsorbed on the Cu atom (Fig. 3g, -1.49 meV); the 17% difference in the MAE is consistent with the experimental changes found for D for Nc on the surface and on the tip. This shows that the MAE is affected by the local ligand field as remarked in other systems.[39]

Finally, to exemplify the effect of having a functionalized Nc tip we acquired IETS spectra above of a Nc molecule adsorbed on the surface using a molecular tip (see Fig. 4a-c). In this case, along with the conductance steps at $\Delta = |3.4 \pm 0.2|$ meV, a new set of prominent steps appears at $|6.9 \pm 0.4|$ meV, which are the signature of a double spin-excitation process

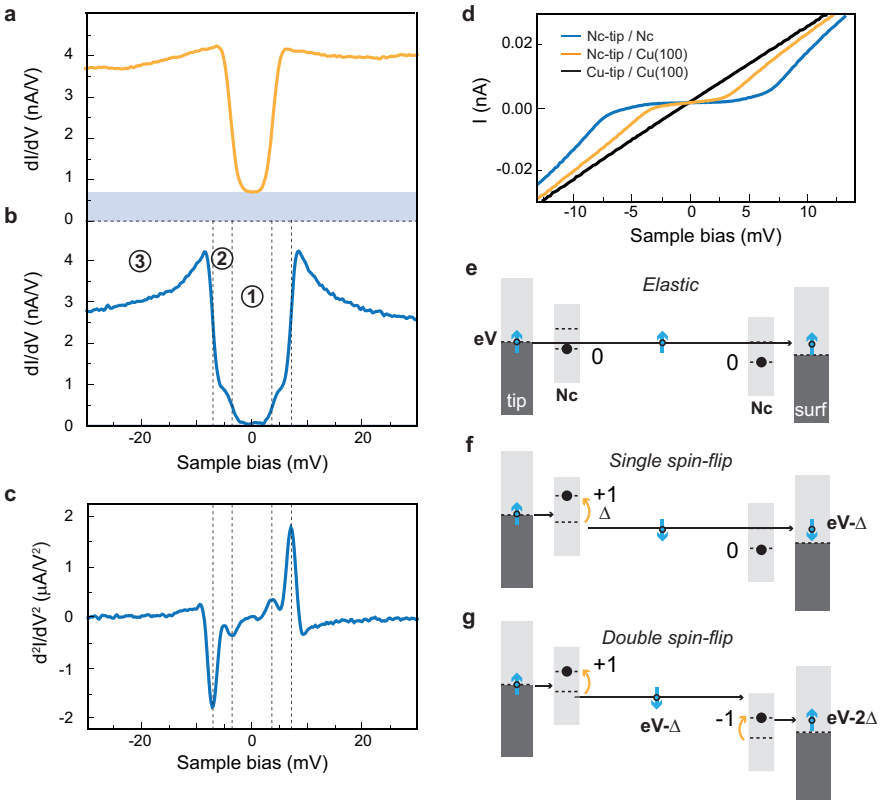

Figure 4: **Double spin-flip excitation.** (a) dI/dV spectrum of a Nc-terminated tip above Cu(100). Panel (b) and (c) show the dI/dV spectrum of a Nc molecule measured with a Nc-terminated tip and its derivative. Three tunneling regimes are highlighted (see text) indicated by regions 1, 2 and 3. To record the spectra the feedback loop was opened at 100 pA and -40 mV. Note that the different elastic background observed in (a) and (b) is due to a larger tip-surface distance in (b). Panel (d) presents the $I(V)$ curve showing the opening of the inelastic channels. Panels (e) to (g) present a sketch of the different tunneling mechanisms: (e) there is only elastic tunneling of electrons; (f) the spin of just one of the molecules is excited. In this case the excitation of the molecule on the tip from $M = 0$ to $M = +1$ is shown, (g) both molecules undergo spin-flip excitations.

sequentially involving the nickelocene on the tip and on the surface, or *vice versa*. These inelastic processes can be directly detected in the $I(V)$ curve shown in Fig. 4d. To explain the origin of these steps, we suppose first, for simplicity, that the molecules on the tip and on the surface have the same threshold energy Δ. When a tunneling electron has an energy below Δ (region 1) only elastic tunneling processes can take place (Fig. 4e). Above that threshold but below 2Δ (region 2), one of the molecular spins, either the one on the tip or the one on the surface, can be excited (Fig. 4f). Above 2Δ (region 3) a tunneling electron has sufficient energy to excite inelastically both molecules (Fig. 4g). Taking now into account the slightly different threshold energies as evidenced above for Nc on the tip (3.7 meV) and on the surface (3.2 meV), we find that their sum nicely matches the threshold energy found for a double excitation. In principle, in region 2 two additional steps (at 3.2 meV and 3.7 meV) rather than one (3.4 meV) should be observed, but their detection is beyond our energy resolution.

The most prominent effect associated to the double spin excitation is the drastic enhancement of the conduction step height observed at 2Δ (a factor 43 with respect the elastic signal in the spectrum of Fig. 4b) that we explain as follows. Let us suppose that the conductance is proportional to the probability of taking one electron from one electrode (tip) into the other electrode (surface), in other words that the conductance is proportional to the T-matrix modulus squared (see Supporting Information). Since the T-matrix has now spin degrees of freedom in the tip and on the sample, we denote the new matrix elements as $T_{n,m}$ where n is the number of excitations of the tip and m the number of excitations of the sample. Then, the conductance will be proportional to $\sum_{n,m} |T_{n,m}|^2$, with a sum on the excitations since the channels are supposed independent. In this case, $T_{0,0}$ corresponds to the elastic transmission of an electron from the tip to the surface or *vice versa* (region 1). $T_{1,0}$ and $T_{0,1}$ correspond to the case in which there is only one inelastic event during the process, i.e., in the molecule on the tip, or on the surface. Finally, $T_{1,1}$ is related to the probability of an electron being transmitted inelastically between the electrodes exciting

both molecules. Hence, if the applied bias is high enough to open the first excitation channel for the molecules on the tip and on the sample (region 3), we obtain that the conductance is proportional to $|T_{0,0}|^2 + |T_{1,0}|^2 + |T_{0,1}|^2 + |T_{1,1}|^2$. The observed inelastic *versus* elastic ratios show tip dependency. Considering the maximum step height values we observed, we have for the Nc on the tip that $(|T_{1,0}|^2 + |T_{0,0}|^2)/|T_{0,0}|^2 \approx 9$ and for the Nc on the surface $(|T_{0,1}|^2 + |T_{0,0}|^2)/|T_{0,0}|^2 \approx 6$. Since the excitations of the molecule on the tip and on the sample are independent, the relative transmission probability of a double spin-flip excitation to occur is approximately $|T_{1,0}|^2|T_{0,1}|^2/|T_{0,0}|^4 = |T_{1,1}|^2/|T_{0,0}|^2 \approx 8 \cdot 5 = 40$. The conductance is then in region 3, $(|T_{0,0}|^2 + |T_{1,0}|^2 + |T_{0,1}|^2 + |T_{1,1}|^2)/|T_{0,0}|^2$=1+6+9+40, this is 56 times higher than the elastic conductance alone (region 1).

To summarize, we have shown how the spin of a nickelocene molecule is preserved in different situations; isolated, self-assembled on a metallic surface or even in the tip apex. The remarkably efficient inelastic spin-flip mechanism exhibited by the molecule has been explained using a T-matrix approach due to the interference effect of the two spin-channel symmetries. The tip-functionalization has been used to trigger a double molecular spin-flip excitation leading to an enhancement of the inelastic signal in spin-flip spectroscopy. On a more fundamental note, the portability of the spin-flip excitations, whether of nickelocene or eventually of other molecules, could serve as a spin-sensitive probe (with or without magnetic field) and thereby provide quantitative spin-dependent STM data.

Methods

Tip and sample preparation

The Cu(100) and Cu(111) samples were cleaned by repeated Ar^+ ion bombardment and annealing at 810 K. The nickelocene (Nc) molecules were deposited onto the copper surfaces by sublimating a nickelocene powder purchased from Sigma-Aldrich. Given the low vapor pressure of nickelocene,[40] the powder sublimation occurs at room temperature in vacuum.

The nickelocene powder was first purified for 5 hours at a pressure close to 10^{-6} mbar; nickelocene deposition was carried out at room temperature in ultra-high vacuum through a gate valve onto the copper surfaces kept at temperatures ranging from 70 to 150 K. The pressure during deposition was $7{\cdot}10^{-10}$ mbar, while the deposition rate was 0.025 monolayer/min. The copper samples were subsequently cooled down to the working temperature.

Inelastic electron tunneling spectroscopy (IETS)

The tunneling spectra were acquired with an ultra-high vacuum scanning tunneling microscope operated at 2.4 K at a base pressure below 10^{-10} mbar. Electrochemically etched W tips were cleaned by Ar-ion sputtering and indented *in vacuo* into the pristine copper surfaces to ensure a flat electronic structure in the bias range of interest. The differential conductance, dI/dV, was measured by means of a lock-in amplifier using a modulation of 150 μV rms at 722 Hz. In order to precisely extract the threshold energy of the spin-flip excitation, we fitted the IETS spectra with the expression of Ref.[41] The d^2I/dV^2 versus V spectra were obtained by numerically deriving the dI/dV spectra.

X-ray magnetic circular dichroism (XMCD)

The XMCD measurements were carried out at the DEIMOS beamline of synchrotron SOLEIL (Saint-Aubin, France) by using circularly polarized light at a temperature ranging from 3.4 to 85 K with a maximum magnetic field of 6.5 T. The samples were prepared following the same procedure used for the STM measurements, using a low coverage within the isolated molecule regime. In our XMCD measurements the applied static magnetic field is parallel to the photon beam direction (fig. S1), which impinges on the sample surface with an angle θ. The angle $\theta = 0°$ defines the normal incidence, and $\theta = 60°$ the grazing incidence. Since isolated nickelocene molecules adsorb with the molecular axis perpendicular to the surface, for simplicity we define the z-axis along the molecular axis. The magnetic field is then in the (x, z) plane.

DFT

Our calculations were done in the framework of Density Functional Theory (DFT) as implemented in the Vienna *ab-initio* Simulation Package (VASP)[42,43] using the projector-augmented wave (PAW)[44] formalism. We adopted the exchange correlation functional with the spin-polarized generalized gradient approximation (GGA)[45] with the PBE[46] form. The wave plane expansion has a kinetic energy cut-off of 800 eV. Partial occupancies were determined by the Methfessel-Paxton scheme considering a smearing of 0.2 eV. The Cu(100) surface was modeled using a supercell built up of five Cu atomic layers and additional vacuum in the Z direction (19 Å), large enough to avoid residual interactions with periodic images. The nickelocene molecule was placed in a 6×6 surface unit cell of Cu(100) with the longer axis perpendicular to the surface, i.e., in a vertical position. The adsorbed Cu atom was placed in a hollow adsorption site according to a previous geometric optimization.[20] The two topmost copper layers, the molecule and the adsorbed Cu atom were allowed to relax until the forces on the individual atoms were less than 0.01 eV Å^{-1} together with an electronic convergence criterion of 10^{-7} eV Å^{-1}. All calculations were performed for the Γ k-point in the first Brillouin zone of the supercell.

To obtain the magnetic anisotropy energy (MAE) within the DFT framework we included the Spin Orbit Coupling (labelled SOC) as implemented in VASP by Kresse and Lebacq.[47] The Magnetic Anisotropy Energy (labelled MAE) is defined as

$$MAE = E_{||}^{SOC} - E_{\perp}^{SOC}, \tag{1}$$

where $E_{||}^{SOC}$ and $E_{\perp}^{SOC}$ correspond to the energy obtained including the spin orbit interaction while considering the spin axis respectively parallel and perpendicular to the metallic surface. Both energies were calculated from a previous relaxed magnetic ground state, with no further relaxation. According to the MAE sign one can distinguish two possible cases. When MAE is positive (negative), the $E_{\perp}^{SOC}$ ($E_{||}^{SOC}$) is more stable yielding a magnetic easy axis along

the perpendicular (parallel) direction with respect to the surface. As the order of magnitude of the MAE value is several times lower than the total energy of the system, the accuracy determining each energy value is crucial. For that reason different calculation parameters such as the energy cut-off, smearing width, and convergence thresholds were thoroughly checked in order to obtain a good compromise between precision and computational effort.

Funding

This work has been supported by the Agence Nationale de la Recherche (Grant No. ANR-13-BS10-0016, ANR-11-LABX-0058 NIE, ANR-10-LABX-0026 CSC). Experiments were performed on the DEIMOS beamline[48] at SOLEIL Synchrotron, France (proposal number 20150309). We are grateful to the SOLEIL staff for smoothly running the facility. We thank the national computational center IDRIS, CINES and TGCC (Grant - [x2015087364]) for CPU time.

Supporting Information Available

Additional information regarding the XMCD measurements and the T-matrix calculation.

This material is available free of charge via the Internet at `http://pubs.acs.org/`.

References

(1) Gatteschi, D.; Sessoli, R.; Villain, J. *Molecular Nanomagnets*; OUP Oxford, 2006.

(2) Leuenberger, M. N.; Loss, D. *Nature* **2001**, *410*, 789–793.

(3) González, G.; Leuenberger, M. N. *Journal of Physics: Condensed Matter* **2014**, *26*, 275302.

(4) Gambardella, P.; Rusponi, S.; Veronese, M.; Dhesi, S. S.; Grazioli, C.; Dallmeyer, A.;

Cabria, I.; Zeller, R.; Dederichs, P. H.; Kern, K.; Carbone, C.; Brune, H. *Science* **2003**, *300*, 1130–1133.

(5) Zyazin, A. S.; van den Berg, J. W. G.; Osorio, E. A.; van der Zant, H. S. J.; Konstantinidis, N. P.; Leijnse, M.; Wegewijs, M. R.; May, F.; Hofstetter, W.; Danieli, C.; Cornia, A. *Nano Lett.* **2010**, *10*, 3307–3311.

(6) Thiele, S.; Balestro, F.; Ballou, R.; Klyatskaya, S.; Ruben, M.; Wernsdorfer, W. *Science* **2014**, *344*, 1135–1138.

(7) Rau, I. G. et al. *Science* **2014**, *344*, 988–992.

(8) Donati, F. et al. *Science* **2016**, *352*, 318–321.

(9) Heinrich, A. J.; Gupta, J. A.; Lutz, C. P.; Eigler, D. M. *Science* **2004**, *306*, 466–469.

(10) Hirjibehedin, C. F.; Lin, C.-Y.; Otte, A. F.; Ternes, M.; Lutz, C. P.; Jones, B. A.; Heinrich, A. J. *Science* **2007**, *317*, 1199–1203.

(11) Chen, X.; Fu, Y.-S.; Ji, S.-H.; Zhang, T.; Cheng, P.; Ma, X.-C.; Zou, X.-L.; Duan, W.-H.; Jia, J.-F.; Xue, Q.-K. *Phys. Rev. Lett.* **2008**, *101*, 197208.

(12) Tsukahara, N.; Noto, K.-i.; Ohara, M.; Shiraki, S.; Takagi, N.; Takata, Y.; Miyawaki, J.; Taguchi, M.; Chainani, A.; Shin, S.; Kawai, M. *Phys. Rev. Lett.* **2009**, *102*, 167203.

(13) Khajetoorians, A. A.; Valentyuk, M.; Steinbrecher, M.; Schlenk, T.; Shick, A.; Kolorenc, J.; Lichtenstein, A. I.; Wehling, T. O.; Wiesendanger, R.; Wiebe, J. *Nat. Nanotech.* **2015**, *10*, 958–964.

(14) Jacobson, P.; Herden, T.; Muenks, M.; Laskin, G.; Brovko, O.; Stepanyuk, V.; Ternes, M.; Kern, K. *Nat. Commun.* **2015**, *6*, 8536.

(15) Loth, S.; von Bergmann, K.; Ternes, M.; Otte, A. F.; Lutz, C. P.; Heinrich, A. J. *Nat. Phys.* **2010**, *6*, 340–344.

(16) Loth, S.; Etzkorn, M.; Lutz, C. P.; Eigler, D. M.; Heinrich, A. J. *Science* **2010**, *329*, 1628–1630.

(17) Yan, S.; Choi, D.-J.; J., B. A.; Rolf-Pissarczyk, S.; Loth, S. *Nat. Nanotech.* **2015**, *10*, 40–45.

(18) Heinrich, B. W.; Braun, L.; Pascual, J. I.; Franke, K. J. *Nat. Phys.* **2013**, *9*, 765 – 768.

(19) Zhen-Feng, X.; Yaoming, X.; Wen-Lin, F.; Henry F., S. *J. Phys. Chem. A* **2003**, *107*, 2716–2729.

(20) Bachellier, N.; Ormaza, M.; Faraggi, M.; Verlhac, B.; Vérot, M.; Le Bahers, T.; Bocquet, M.-L.; Limot, L. *Phys. Rev. B* **2016**, *93*, 195403.

(21) Pugmire, D.; Woodbridge, C.; Boag, N.; Langell, M. *Surf. Sci.* **2001**, *472*, 155 – 171.

(22) Miyamachi, T. et al. *Nature* **2013**, *503*, 242–246.

(23) Ormaza, M.; Abufager, P.; Bachellier, N.; Robles, R.; Verot, M.; Le Bahers, T.; Bocquet, M.-L.; Lorente, N.; Limot, L. *J. Phys. Chem. Lett.* **2015**, *6*, 395.

(24) Prins, R.; van Voorst, J.; Schinkel, C. *Chem. Phys. Lett.* **1967**, *1*, 54 – 55.

(25) Baltzer, P.; Furrer, A.; Hulliger, J.; Stebler, A. *Inorg. Chem.* **1988**, *27*, 1543–1548.

(26) Li, S.; Hamrick, Y. M.; Zee, R. J. V.; Jr., W. W. *J. Am. Chem. Soc.* **1992**, *114*, 4433–4434.

(27) Vaara, J.; Rouf, S. A.; Mare, J. *J. Chem. Theory Comput.* **2015**, *11*, 4840–4849.

(28) Wagner, C.; Temirov, R. *Progress in Surface Science* **2015**, *90*, 194 – 222.

(29) Chiang, C.-l.; Xu, C.; Han, Z.; Ho, W. *Science* **2014**, *344*, 885–888.

(30) Hapala, P.; Kichin, G.; Wagner, C.; Tautz, F. S.; Temirov, R.; Jelínek, P. *Phys. Rev. B* **2014**, *90*, 085421.

(31) Temirov, R.; Soubatch, S.; Neucheva, O.; Lassise, A. C.; Tautz, F. S. *New Journal of Physics* **2008**, *10*, 053012.

(32) Weiss, C.; Wagner, C.; Kleimann, C.; Rohlfing, M.; Tautz, F. S.; Temirov, R. *Phys. Rev. Lett.* **2010**, *105*, 086103.

(33) Gross, L.; Mohn, F.; Moll, N.; Liljeroth, P.; Meyer, G. *Science* **2009**, *325*, 1110–1114.

(34) Eigler, D.; Lutz, C.; Rudge, W. *Nature* **1991**, *352*, 600 – 603.

(35) Bartels, L.; Meyer, G.; Rieder, K.-H.; Velic, D.; Knoesel, E.; Hotzel, A.; Wolf, M.; Ertl, G. *Phys. Rev. Lett.* **1998**, *80*, 2004–2007.

(36) Wagner, C.; Green, M. F. B.; Leinen, P.; Deilmann, T.; Krüger, P.; Rohlfing, M.; Temirov, R.; Tautz, F. S. *Phys. Rev. Lett.* **2015**, *115*, 026101.

(37) Ormaza, M.; Robles, R.; Bachellier, N.; Abufager, P.; Lorente, N.; Limot, L. *Nano Lett.* **2016**, *16*, 588–593.

(38) Heinrich, B. W.; Rastei, M. V.; Choi, D.-J.; Frederiksen, T.; Limot, L. *Phys. Rev. Lett.* **2011**, *107*, 246801.

(39) Heinrich, B. W.; Braun, L.; Pascual, J. I.; Franke, K. J. *Nano Lett.* **2015**, *15*, 4024–4028.

(40) Vieyra-Eusebio, M. T.; Rojas, A. *J. Chem. Eng. Data* **2011**, *56*, 5008–5018.

(41) Lambe, J.; Jaklevic, R. C. *Phys. Rev.* **1968**, *165*, 821–832.

(42) Kresse, G.; Furthmüller, J. *Comput. Mater. Sci.* **1996**, *6*, 15.

(43) Kresse, G.; Joubert, D. *Phys. Rev. B* **1999**, *59*, 1758.

(44) Blöchl, P. E. *Phys. Rev. B* **1994**, *50*, 17953.

(45) Perdew, J. P.; Chevary, J. A.; Vosko, S. H.; Jackson, K. A.; Pederson, M. R.; Singh, D. J.; Fiolhais, C. *Phys. Rev. B* **1992**, *46*, 6671–6687.

(46) Perdew, J. P.; Burke, K.; Ernzerhof, M. *Phys. Rev. Lett.* **1996**, *77*, 3865.

(47) Kresse, G.; Lebacq, O. VASP manual. `http://cms.mpi.univie.ac.at/vasp/`.

(48) Ohresser, P. et al. *Rev. Sci. Instr.* **2014**, *85*.